Supporting Information for

Visible Light-Driven Water Oxidation with Subporphyrin Sensitizer and Water Oxidation Catalyst

Masanori Yamamoto,[†] Yusuke Nishizawa,[†] Pavel Chábera,[‡] Fusheng Li,[‖] Torbjörn Pascher,[‡] Villy Sundström,*[,‡] Licheng Sun,*[,‖] and Hiroshi Imahori*[,†,¶]

[†]*Department of Molecular Engineering, Graduate School of Engineering, Kyoto University, Nishikyo-ku, Kyoto 615-8510, Japan*
[‡]*Department of Chemical Physics, Lund University, Box 124, 22100 Lund, Sweden*
[‖]*Department of Chemistry, School of Chemical Science and Engineering, Royal Institute of Technology (KTH), 100 44 Stockholm, Sweden*
[¶]*Institute for Integrated Cell-Material Sciences (WPI-iCeMS), Kyoto University, Nishikyo-ku, Kyoto 615-8510, Japan*

E-mail: villy.sundstrom@chemphys.lu.se, lichengs@kth.se, imahori@scl.kyoto-u.ac.jp

Contents

S1. General Information for Experiments

Materials and General Procedures. Tetrahydrofuran and triethylamine were distilled from CaH_2. Other solvents and chemicals were of reagent-grade quality, purchased commercially and used without further purification unless otherwise noted. Column chromatography and thin-layer chromatography (TLC) were performed with UltraPure Silica Gel (230 − 400 mesh, SiliCycle Inc.) and Silica gel 60 F_{254} (Merck), respectively. Melting points were recorded on a Yanagimoto micro-melting point apparatus and not corrected. TiO_2 electrodes for electrochemical measurements were prepared by doctor blade techniques, while TiO_2 electrodes for photoelectrochemical and transient absorption measurements were prepared by screen printing techniques as previously reported.[S1]

Electrochemical Measurements. Cyclic voltammetry (CV) and differential pulse voltammetry (DPV) were performed on an ALS660A electrochemical analyzer in deaerated sodium phosphate buffered aqueous solution (NaPi, pH 7.3, 0.1 M, 1.87 g of NaH_2PO_4 and 6.45 g of Na_2HPO_4 in 300 mL of water) or deaerated dichloromethane containing 0.1 M of tetrabutylammonium hexafluorophosphate ($TBAPF_6$). A conventional three-electrode cell consisted of a modified FTO/TiO_2 working electrode (or a glassy carbon working electrode), a Ag/AgCl (3 M NaCl aqueous solution) reference electrode, and a Pt wire counter electrode. The measured potentials were recorded with respect to the reference electrode, and redox potentials were reported according to following equation: $E_{\mathrm{NHE}} = E_{\mathrm{Ag/AgCl}} + 0.207$ V.[S2]

Photoelectrochemical Measurements. Photoelectrochemical measurements were performed using an ALS660A electrochemical analyzer and the standard three-electrode electrochemical cell with the FTO/TiO_2/**SP**+**RuWOC**, FTO/TiO_2/**SP**, or FTO/TiO_2/**RuWOC** working electrode, the Pt wire counter electrode, and the Ag/AgCl (3 M NaCl aqueous solution) reference electrode. The photocurrent was measured at 0.207 vs NHE without stirring and iR compensation.[S3] A 100 W halogen lamp (MEJIRO PRECISION, PHL-100) coupled with a 380 nm long-pass filter was used as a white light source ($\lambda_{\mathrm{ex}} > 380$ nm; input power, 100 mW cm^{-2}) for the DSPEC with I^-/I_3^- redox couple (A Pt wire covered with a glass ruggin capillary, whose tip was located near the working electrode and a Pt coil were used an quasireference and counter electrodes, respectively). An LED Light Source (Hayashi Watch-Works Co., Ltd, LA-HDF158AS) was used as a white light source ($\lambda_{\mathrm{ex}} > 420$ nm) for the photoelectrochemical water oxidation analysis. A 500 W Xe lamp (USHIO, XB-50101AAA) was used for the IPCE measurements. A 300 W Xe lamp (Asahi Spectra Co., Ltd., MAX-303) coupled with a 400 nm long-pass filter was used as a white light source ($\lambda_{\mathrm{ex}} > 400$ nm) for the long-term photolysis of water. Monochromatic light was obtained through a monochromator (Ritsu, MC-10N) and used to illuminate the modified area of the working electrode (0.28 cm^2). The light intensity was monitored by an optical power meter (Anritsu, ML9002A) and corrected to calculate the IPCE values.

XPS. The data were collected using a ULVAC-PHI 5500MT instrument with a Mg Kα X-ray source (1253.6 eV) and a hemispherical energy analyzer as previously reported.[S1] The spectra were reported with reference to the In $3d_{5/2}$ peak of In foil as an internal reference with a binding energy of 443.8 eV.

S2. Quantum Chemical Calculations

Gas phase DFT calculations on **SP** were carried out using the Gaussian 03 package of program[S4] with the B3LYP functional and the 3−21G basis set, followed by the 6−311++G(d,p) basis set, which is often used for calculations involving push−pull type molecules.[S5] The frequency analyses were carried out at the same level. The molecular orbitals were visualized by Molstudio 3.0 software.

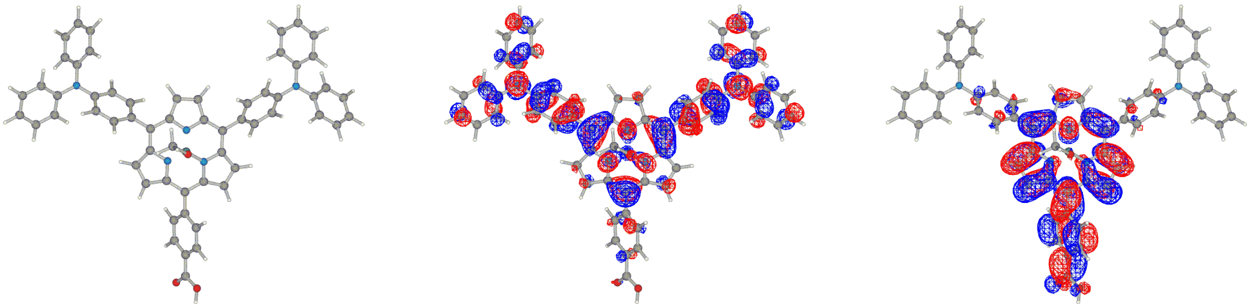

Figure S1. Structure and the selected molecular orbitals of the push−pull **SP** calculated at the B3LYP/6−311++G(d,p) level of theory. (left) The optimized structure, (center) Kohn−Sham highest occupied molecular orbital (HOMO), and (right) lowest unoccupied molecular orbital (LUMO) of **SP**. White: hydrogen, green: boron, gray: carbon, blue: nitrogen, and red: oxygen. The dihedral angle between the *meso*-phenyl ring and the macrocycle plane was 48.8 − 55.2 °, thus achieving an efficient expansion of the π-system.

As shown in Figure S2, the TD-DFT calculation at the B3LYP/6-311++G(d,p) level of theory predicted that a lowest-energy transition with an oscillator strength of 0.2055 would occur at 511 nm with 80% HOMO-to-LUMO transition and 20% HOMO−3-to-LUMO+1 transition. The theoretical simulation is in good agreement with the experimental UV-vis absorption spectrum of **SP** (Figure S7), supporting the electronic structure of the push−pull sensitizer.

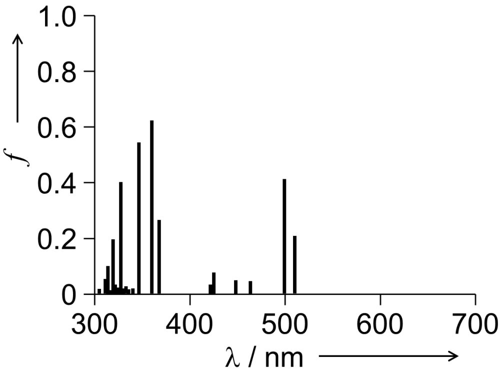

Selected transitions of **SP** simulated by TD-DFT.

	λ / nm	transition		*f*
1	511.44	HOMO−3 to LUMO+1	0.16240	0.2055
		HOMO to LUMO	0.67620	
2	500.39	HOMO−3 to LUMO	−0.17456	0.4068
		HOMO−1 to LUMO	−0.10028	
		HOMO to LUMO+1	0.66718	
3	358.22	HOMO−3 to LUMO	0.39770	0.6399
		HOMO−3 to LUMO+1	0.18108	
		HOMO−3 to LUMO+2	0.15755	
		HOMO−2 to LUMO	−0.15327	
		HOMO−2 to LUMO+1	0.44307	
		HOMO to LUMO+8	0.10625	

Figure S2. Calculated transition of **SP** by TD-DFT at the B3LYP/6−311++G(d,p) level of theory. The atom configuration shown in Figure S1 was used for this calculation.

S3. Synthesis and Characterization

RuWOC was prepared according to the literature.[S6] **SP** was synthesized as follows (Scheme S1):[S7] The structure was verified by spectroscopic analyses including ^{1}H, ^{11}B, and ^{13}C{^{1}H} NMR, ESI-HRMS, IR, steady-state absorption and emission spectra, fluorescence lifetime, and electrochemical measurements.

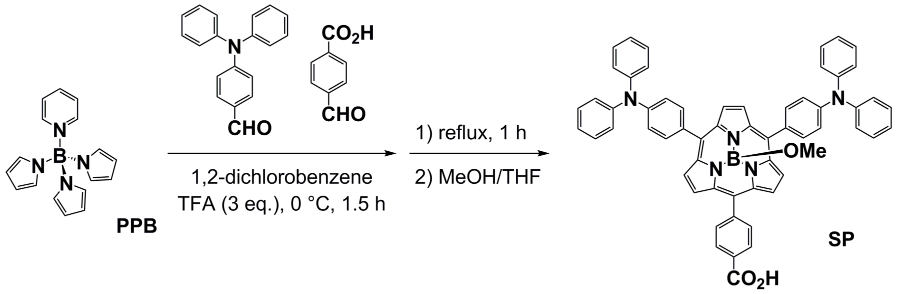

Scheme S1. Synthesis of the push−pull contracted porphyrin, **SP**.

Synthesis of SP: A flask containing pyridine-tri-*N*-pyrrolylborane[S8] (PPB, 1.01 g, 3.50 mmol), 4-(diphenylamino)benzaldehyde (1.91 g, 6.99 mmol), and 4-formylbenzoic acid (0.520 g, 3.46 mmol) in 1,2-dichlorobenzene (130 mL) was degassed for 20 min at 0 °C, and trifluoroacetic acid (TFA, 0.87 mL, 11 mmol) was added dropwise via a syringe. After stirring at 0 °C for 1.5 h under Ar, pyridine (0.86 mL, 11 mmol) was added to the reaction mixture, and the resulting solution was heated to reflux. After stirring for 1 h, the solution was cooled to room temperature, and the solvent was removed in vacuo. The black tar residue was dissolved in 200 mL of tetrahydrofuran/methanol (v/v = 1/1) and stirred at 50 °C for 10 min. The solvent was then evaporated, and the crude mixture was purified on a silica gel column chromatography with dichloromethane/acetone = 3/1, then 5/1 as an eluent. After recrystallization from dichloromethane/methanol/hexane, **SP** was obtained as an orange crystalline solid (13.8 mg, 15.7 μmol, 0.5%). m.p. >300 °C; ^{1}H NMR (600 MHz) in CD_2Cl_2/CD_3OD (v/v = 4/1) with a drop of CD_3CO_2D: δ 8.34 (d, *J* = 8.4 Hz, 2H), 8.21 (d, *J* = 4.2 Hz, 2H), 8.20 (s, 2H), 8.13 (d, *J* = 8.4 Hz, 2H), 8.11 (d, *J* = 4.2 Hz, 2H), 7.92 (d, *J* = 8.4 Hz, 4H), 7.35–7.32 (m, 12H), 7.24 (d, *J* = 8.4 Hz, 8H), 7.09 (t, *J* = 7.5 Hz, 4H); ^{11}B NMR (193 MHz) in CD_2Cl_2/CD_3OD (v/v = 4/1) with a drop of CD_3CO_2D: δ −15.2 (s, 1B); ^{13}C{^{1}H} NMR (151 MHz) in CD_2Cl_2/CD_3OD (v/v = 4/1) with a drop of CD_3CO_2D: δ 148.6, 148.0, 142.3, 141.2, 141.1, 140.9, 134.3, 133.4, 130.7, 130.5, 129.9, 125.5, 124.0, 123.3, 123.2, 122.8, 122.3, 121.6; HRMS (ESI): m/z calcd for $C_{58}H_{39}BN_5O_2$ 848.3191 $[M-OMe]^+$; found: 848.3201; IR (neat): 1714 cm^{-1}; UV/Vis (THF): λ_{max} (ε) = 356 (33 600), 400 (70 200), 510 nm (19 300 M^{-1} cm^{-1}).

S4. NMR of the Push−pull Contracted Porphyrin

^{1}H, ^{11}B, and ^{13}C{^{1}H} NMR spectra were measured on a JNM-ECA600 (JEOL, Japan) spectrometer, and the chemical shifts were recorded relative to the internal reference of tetramethylsilane (0.00 ppm) for ^{1}H, the external reference of borane trifluoride (0.00 ppm) in dichloromethane-d_2 for ^{11}B, and the internal reference of dichloromethane (53.8 ppm) for ^{13}C{^{1}H}.

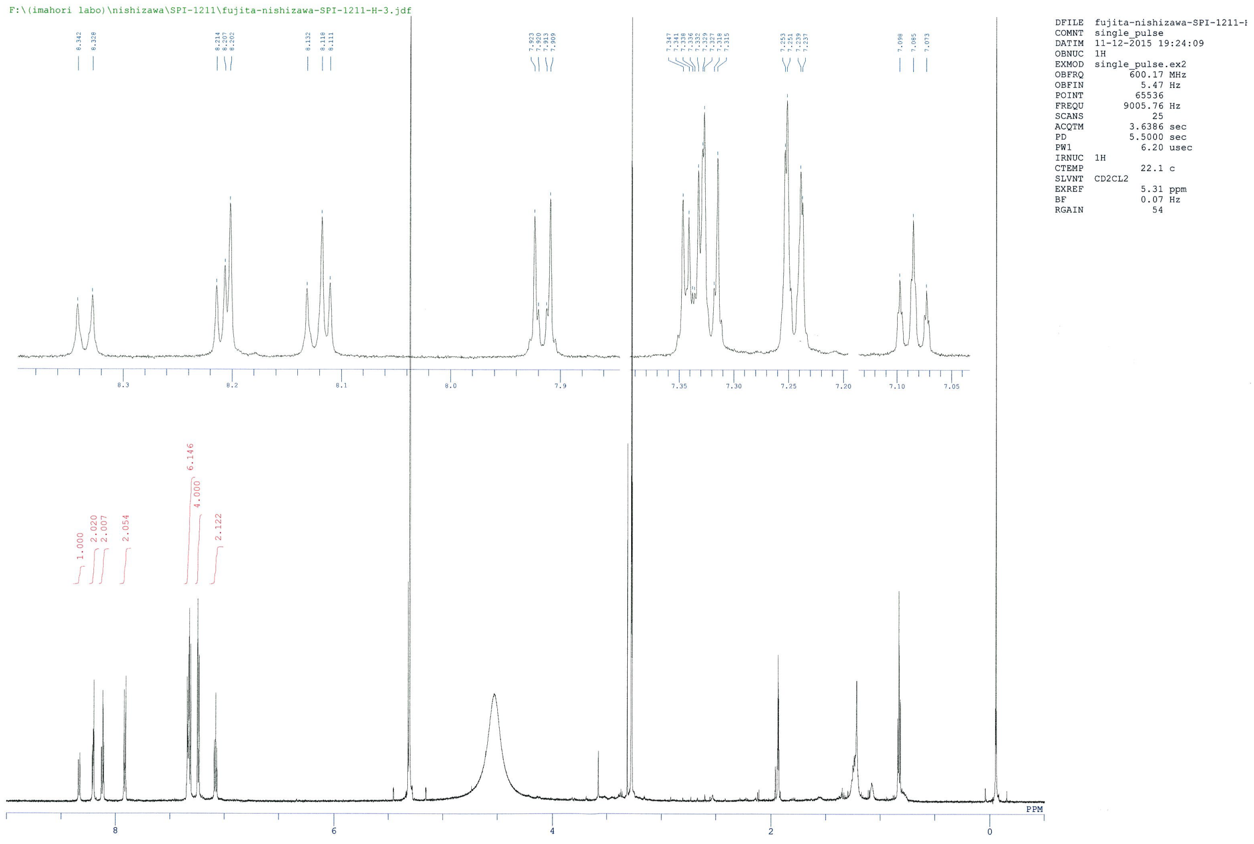

```
DFILE  fujita-nishizawa-SPI-1211-
COMNT  single_pulse
DATIM  11-12-2015 19:24:09
OBNUC  1H
EXMOD  single_pulse.ex2
OBFRQ        600.17 MHz
OBFIN          5.47 Hz
POINT         65536
FREQU       9005.76 Hz
SCANS            25
ACQTM        3.6386 sec
PD           5.5000 sec
PW1            6.20 usec
IRNUC  1H
CTEMP          22.1 c
SLVNT  CD2CL2
EXREF          5.31 ppm
BF             0.07 Hz
RGAIN            54
```

Figure S3. ^{1}H NMR (600 MHz) spectrum of **SP** in CD_2Cl_2/CD_3OD (v/v = 4/1) with a drop of CD_3CO_2D at 295 K. Because of the axial ligand exchange via the subporphyrin borenium cation under acidic conditions,[S9] the proton signals of the methoxy group were not observed.

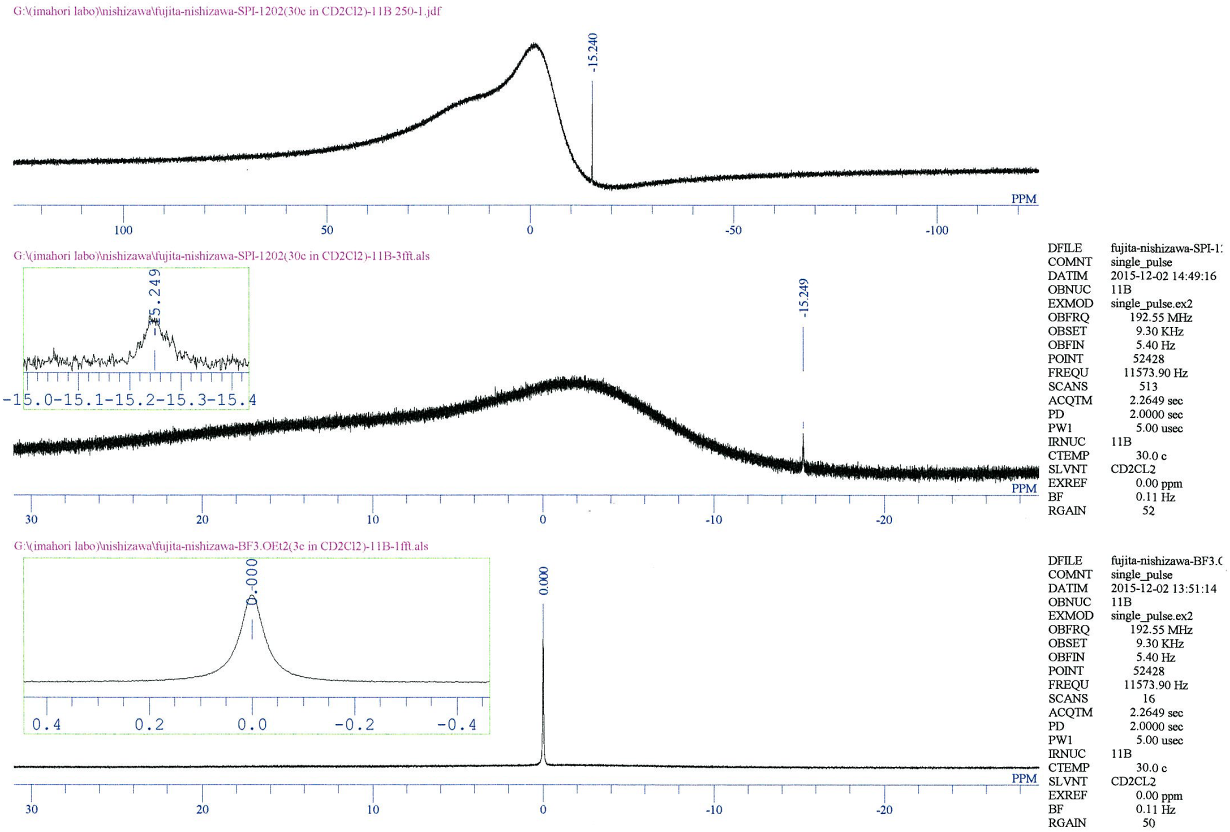

Figure S4. ^{11}B NMR (193 MHz) spectra of **SP** in CD_2Cl_2/CD_3OD (v/v = 4/1) with a drop of CD_3CO_2D (top and middle) and borane trifluoride in CD_2Cl_2 (bottom) at 303 K.

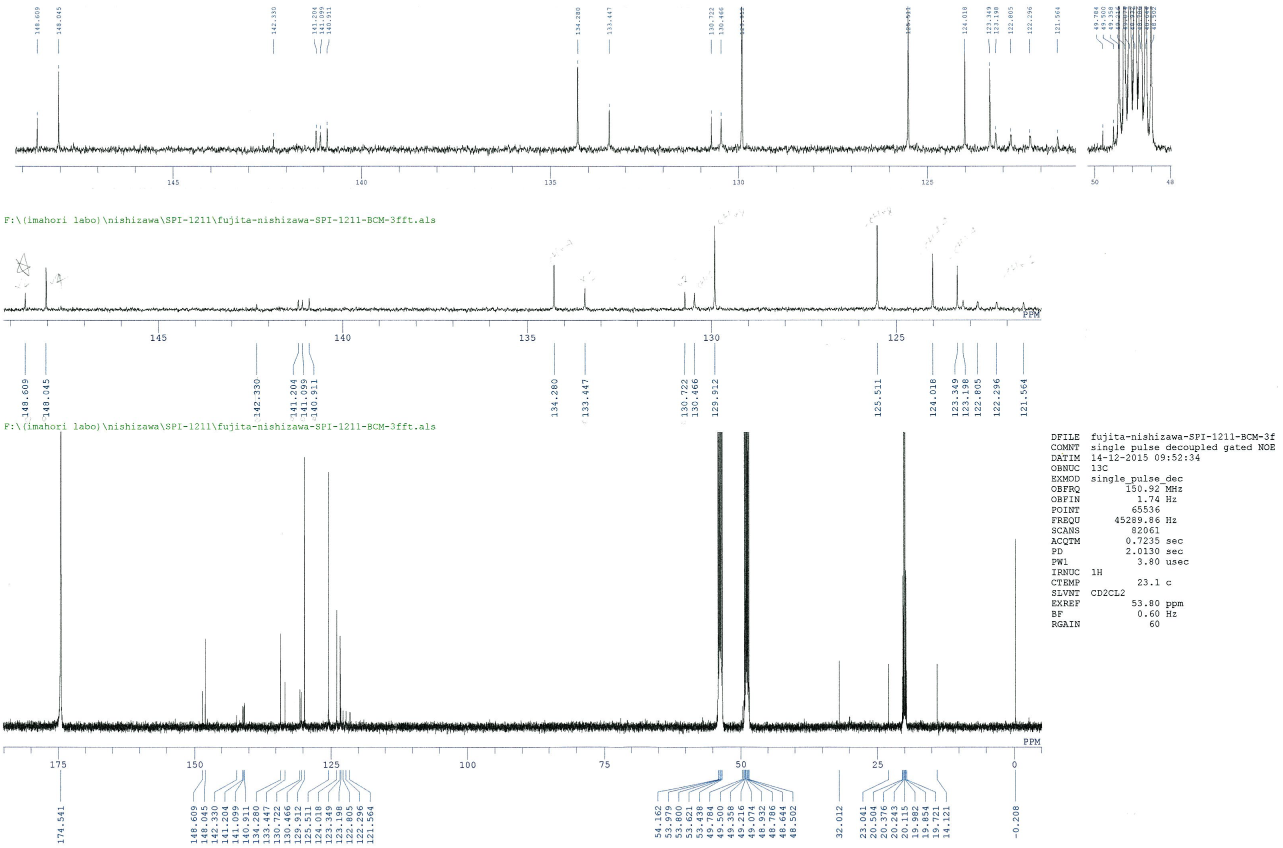

Figure S5. $^{13}C\{^1H\}$ NMR (151 MHz) spectrum of **SP** in CD_2Cl_2/CD_3OD (v/v = 4/1) with a drop of CD_3CO_2D at 296 K.

S5. HRMS of the Push−pull Contracted Porphyrin

ESI-HRMS were obtained on a Thermo Fischer Scientific EXACTIVE spectrometer.

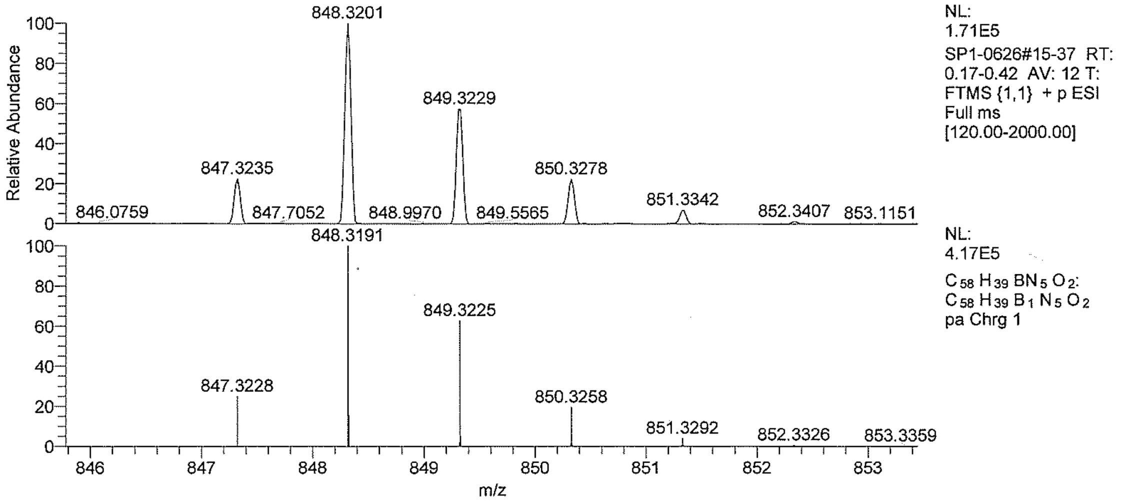

Figure S6. ESI-HRMS of **SP** (top) and simulation pattern calculated for [M−OMe]$^+$ (bottom).

S6. Optical Properties of the Push−pull Contracted Porphyrin

UV-vis absorption spectra were measured with a Lambda 900 (Perkin-Elmer) UV/vis/NIR spectrometer with a data interval of 0.5 nm. Steady-state fluorescence spectra were measured with a FluoroMax-3 (JOBIN YVON, HORIBA) spectrofluorophotometer with a data interval of 1 nm. Time-correlated single-photon-counting was recorded on a HORIBA Jobin Yvon FluoroCube Fluorescence Lifetime System equipped with NanoLEDs and LDs. Hamamatsu (R3809 U) photomultiplier and a thermoelectrically cooled TBX-04-D detector was used to detect the emitted photons. These spectra were taken in ca. 10^{-5}–10^{-6} M solutions in a quartz cell with a path length of 1 cm.

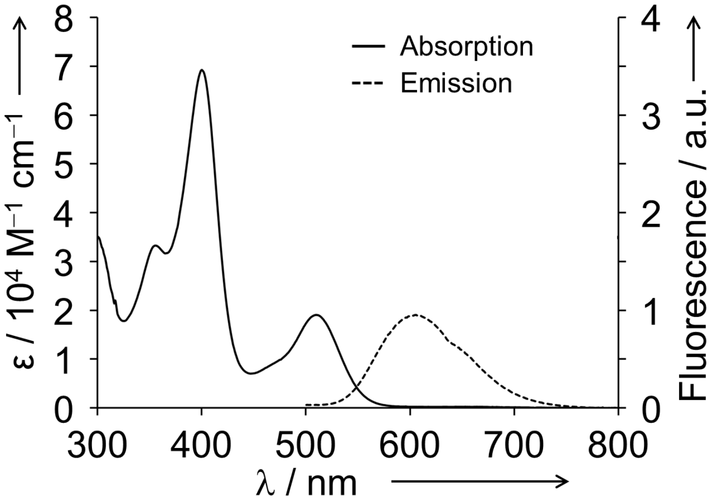

Figure S7. UV-vis absorption (solid) and fluorescence spectra (dashed) of **SP** in methanol. Excitation wavelength: 400 nm. The spectra showed a large Stokes shift, indicating the large structural change of the macrocycle in the excited states.[S10]

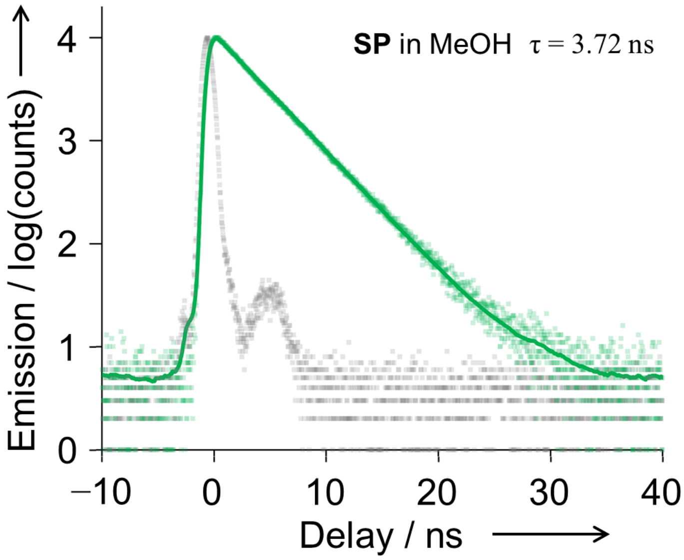

Figure S8. Time-correlated single photon counting of **SP** in methanol at 298 K (green trace) and the fitted line with a lifetime (τ_f) of 3.72 ns (green line). The gray trace is the instrumental response function (IRF). Excitation wavelength: 416 nm. Monitor wavelength: 605 nm.

S7. Electrochemical Properties of the Push−pull Contracted Porphyrin

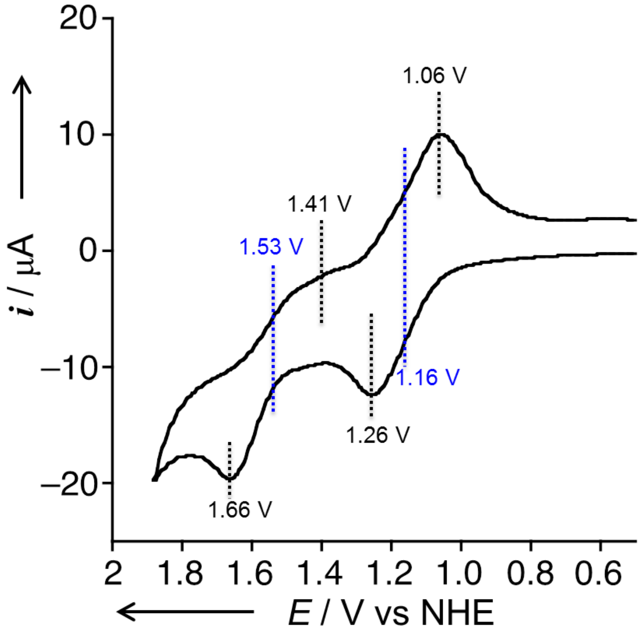

Figure S9. Cyclic voltammogram of **SP** in deaerated dichloromethane containing 0.1 M $TBAPF_6$. Scan rate: 100 mV s^{-1}.

S8. Photoanodes (FTO/TiO_2/SP) Characterization

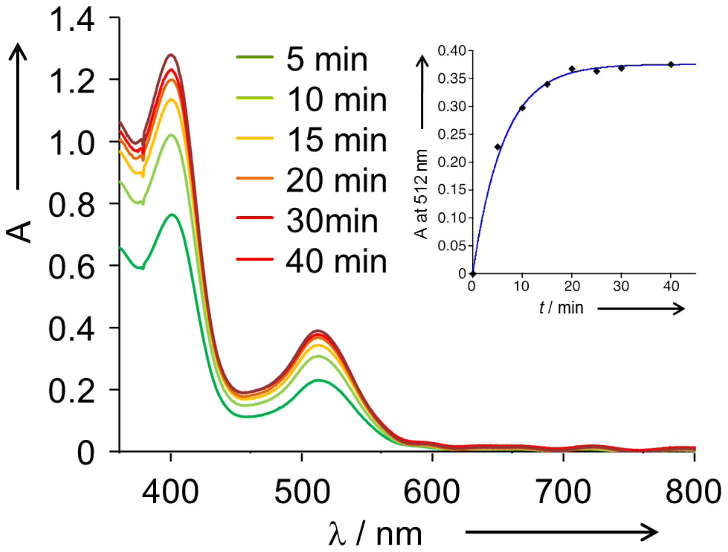

Figure S10. Time course of **SP** adsorption on the surface of an FTO/TiO_2 electrode. Stock solution: 0.18 mM SP in THF/EtOH (v/v = 7:3). The TiO_2 electrodes were prepared by screen printing techniques, and the TiO_2 thickness was 2 μm.

Meyer's method. The surface loading of molecules on the surface of the FTO/TiO_2 electrode (Γ_0') was determined using the following equation:[S11]

$$\Gamma_0{}' = \frac{A_\lambda}{\epsilon_\lambda \times 10^3}\ \mathrm{mol\ cm^{-2}} \qquad \text{(S1)}$$

where A_λ is the absorbance of the electrode and ε_λ is the molar extinction coefficient of the molecules at the wavelength in solution.

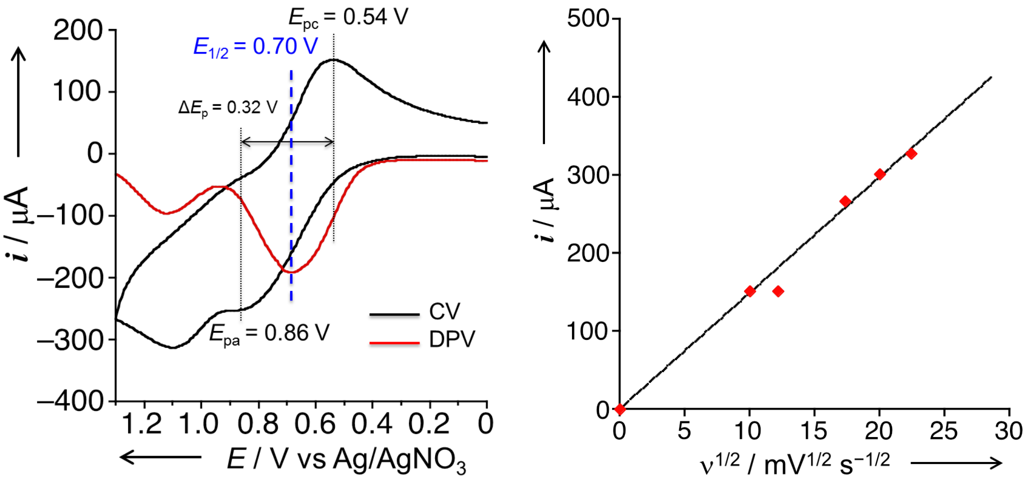

Figure S11. (left) CV and DPV of the FTO/TiO_2/**SP** electrode in deaerated dichloromethane containing 0.1 M $TBAPF_6$. Scan rate: 100 mV s^{-1}. (right) Cathodic current at 0.54 V-square root of the scan rate plot for the electrode when all conditions were the same except for the scan rate. The TiO_2 electrodes were prepared by doctor blade techniques, and the thickness of the TiO_2 film was 9 − 10 μm.

S9. Photoelectrochemical Properties of the FTO/TiO$_2$/SP Electrode under the Three-electrode Setup

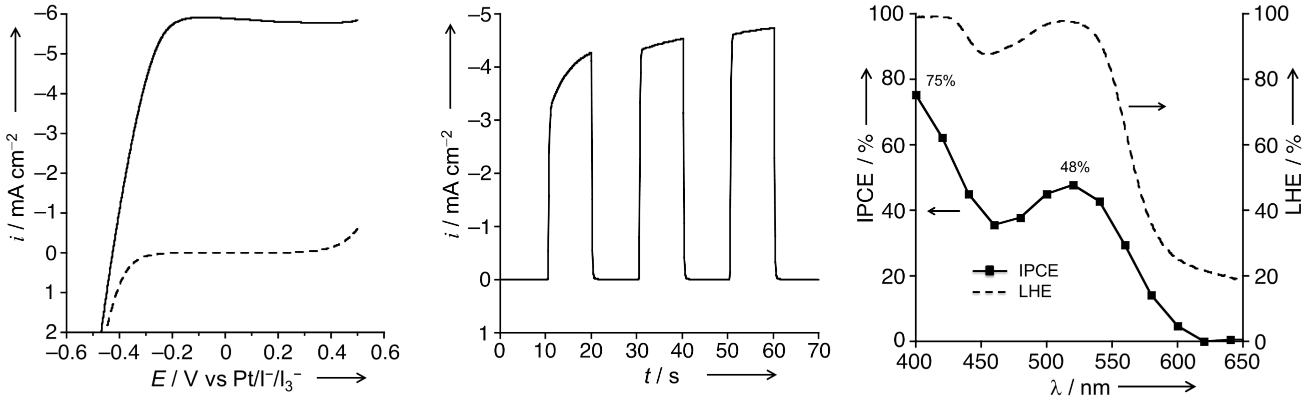

Figure S12. (left) Current density vs potential curve of the FTO/TiO$_2$/**SP** electrode (TiO$_2$ thickness: 12 μm) under white light illumination (input power of 100 mW cm^{-2}, λ_{ex} > 380 nm, solid line) and in the dark (dashed line). (center) Current density vs time curve under white light illumination. (right) Photocurrent action spectra (solid) and LHEs (dashed) of the photoanodes. Conditions: counter electrode: Pt wire; reference electrode: Pt coil; external bias: 0.207 V vs NHE; electrolyte: 0.1 M LiI and 0.05 M I_2 in acetonitrile (I^-/I_3^- redox couple).

S10. Preparation and Characterization of Photoanodes (FTO/TiO$_2$/SP+RuWOC)

The SP-sensitized TiO$_2$ electrode was immersed into an ethanol solution of **RuWOC** (0.34 mM) for 1 min at 298 K (Figures S13 and S14). The electrode was then washed several times with ethanol and water and dried in the dark at room temperature to yield the working photoanode of FTO/TiO$_2$/**SP**+**RuWOC**.

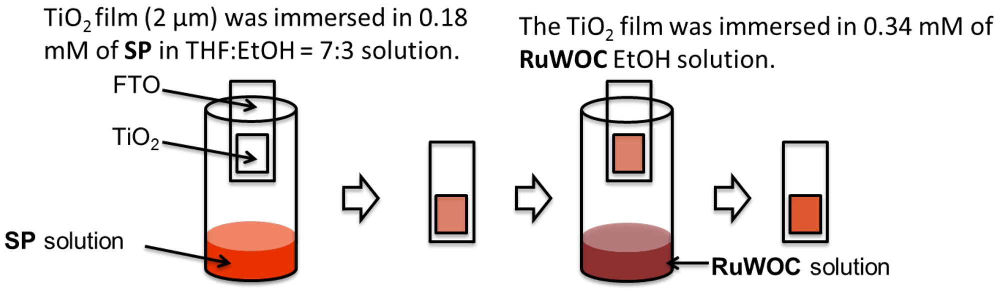

Figure S13. Schematic illustration of the preparation of the FTO/TiO$_2$/**SP**+**RuWOC** electrode.

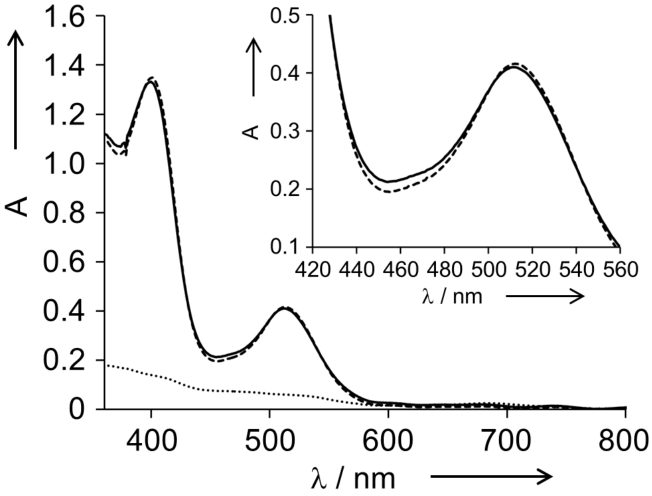

Figure S14. UV-vis absorption spectra of FTO/TiO_2/**SP**+**RuWOC** (solid), FTO/TiO_2/**SP** (dashed), and FTO/TiO_2/**RuWOC** (dotted) electrodes.

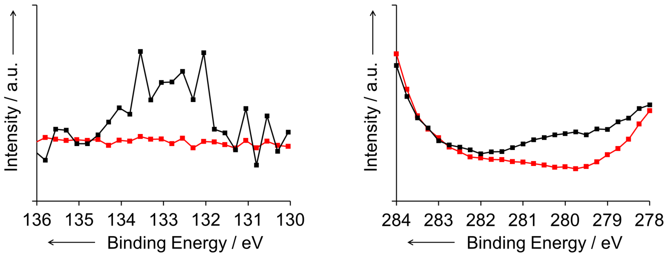

Figure S15. XPS of the FTO/TiO_2/**SP**+**RuWOC** (black) and FTO/TiO_2/**SP** (red) electrodes in the P 2p (left) and Ru $3d_{5/2}$ regions (right). The presence of P (binding energy of 133 eV) and Ru (binding energy of 280 eV) atoms on the surfaces was confirmed.

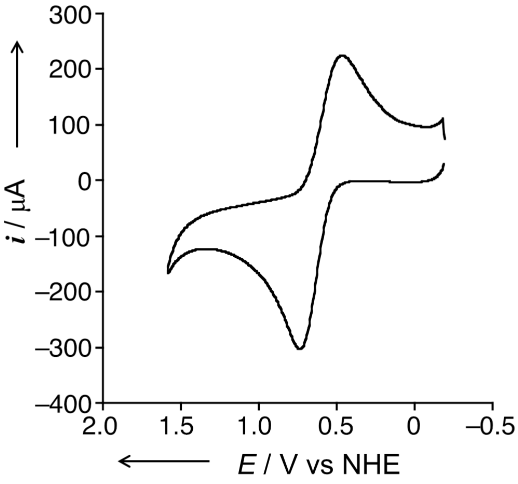

Figure S16. CV of the FTO/TiO_2/**RuWOC** electrode in the aqueous NaPi solution (0.1 M, pH 7.3). Scan rate: 100 mV s^{-1}. The TiO_2 film with a TiO_2 thickness of 9 − 10 µm was prepared by doctor blade technique.

S11. Photoelectrochemical Water Oxidation

Current data upon irradiation were collected in the three-electrode electrochemical cell with the Pt wire counter electrode and the Ag/AgCl reference electrode. The photolysis was performed at 0.207 vs NHE without stirring and iR compensation.[S3]

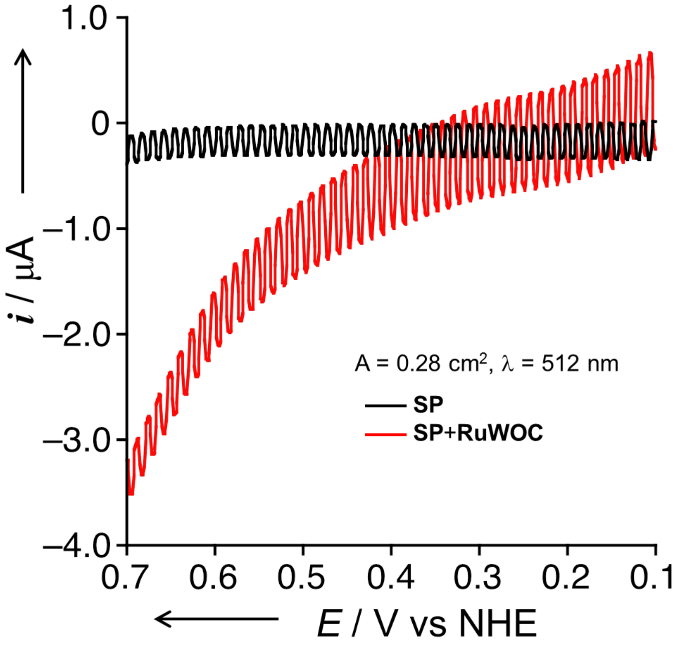

Figure S17. Current vs potential curves of the FTO/TiO_2/**SP** (black) and FTO/TiO_2/**SP**+**RuWOC** (red) electrodes in the aqueous NaPi solution (0.1 M, pH 7.3) under 0.5 Hz chopped green light illumination (512 nm, W_{input} = 0.31 mW cm^{-2}) and in the dark. The TiO_2 electrodes were prepared by screen printing techniques, and the TiO_2 thickness was 2 µm.

Both the photocurrent and the dark current of the FTO/TiO_2/**SP**+**RuWOC** electrode increased significantly at approximately 0.6 V vs NHE (Figure S17). This corresponds to a redox peak of the $\mathrm{Ru^{III}/Ru^{II}}$ pair, supporting the attachment of **RuWOC** on the surfaces of TiO_2.

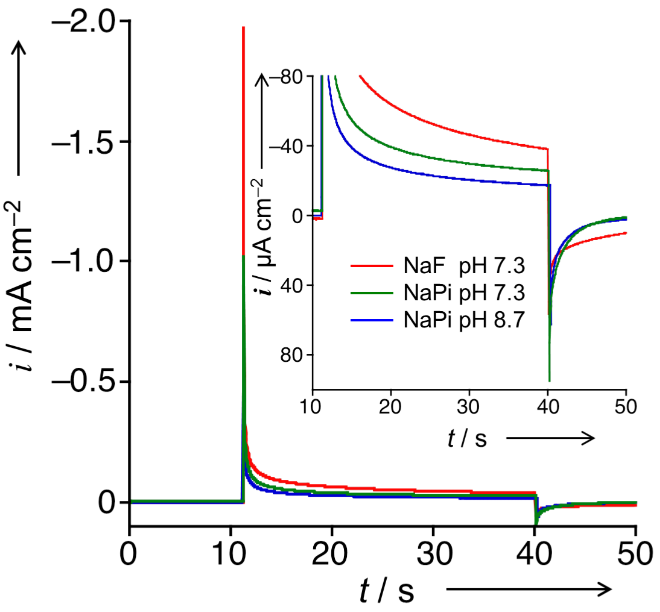

Figure S18. Current density vs time curves of the FTO/TiO_2/**SP**+**RuWOC** electrodes in the various aqueous solutions (electrolyte concentration: 0.1 M) with different pH under white light illumination (λ_{ex} > 420 nm, 100 mW cm^{-2}). The TiO_2 electrodes were prepared by screen printing techniques, and the TiO_2 thickness was 2 µm.

S12. Gas Detection

Analytical GC was performed using a Shimadzu GC-2014 instrument with a thermal conductivity detector (TCD-2014). A molecular sieve column was used as the stationary phase, and Ar gas was employed as the mobile phase. The Ar flow rate was 25 mL min^{-1}, and the column temperature was 40 °C. Aliquots (500 μL) of gas from the headspaces of the DSPECs (25 mL) after the measurements were delivered to the GC system using a Hamilton SampleLock syringe to quantitatively analyze the O_2 and H_2 evolution. A FireSting Oxygen Monitor (BAS Inc.) was used for the time-course measurement of O_2 evolution. Ar containing 10% O_2 purchased from Sumitomo Seika Chemicals Co., Ltd. (Lot No. JTC1520066) was used for the calibration.

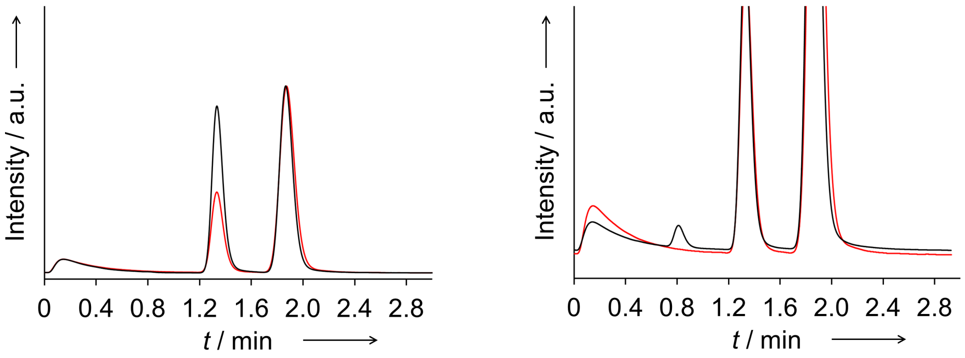

Figure S19. Gas chromatograms of the photoanode compartment (left) and cathode compartment (right) after photolysis under white light illumination (black trace, 100 mW cm^{-2}; photoanode active area: 0.38 cm^{2}) and background air (red trace). Retention time: 0.85 min for H_2, 1.35 min for O_2, 1.9 min for N_2.

S13. Photolysis of $H_2{}^{18}O$ and $^{18}O_2$ Detection by GC-MS

^{18}O-labeled water ($H_2{}^{18}O$, 98 atom%) was purchased from Rotem Industries Ltd. (Lot No.: 15-1257), and used as 0.1 M NaF solution for the photolysis experiments. GC-MS spectra were collected on Bruker SCION SQ 436-GC. Bruker BR-Swax (length: 30 m, diameter: 0.25 mm) was used as the stationary phase, and He gas was employed as the mobile phase. The He flow rate was 1.3 mL min^{-1}, and the column temperature was 40 °C. The split ratio was 20, and the mass spectra were obtained with m/z values from 20 to 120. Aliquots (500 μL) of gas from the headspaces of the PECs (25 mL) after the measurements were delivered to the GC-MS system using a Hamilton SampleLock syringe to qualitatively analyze the evolved gases.

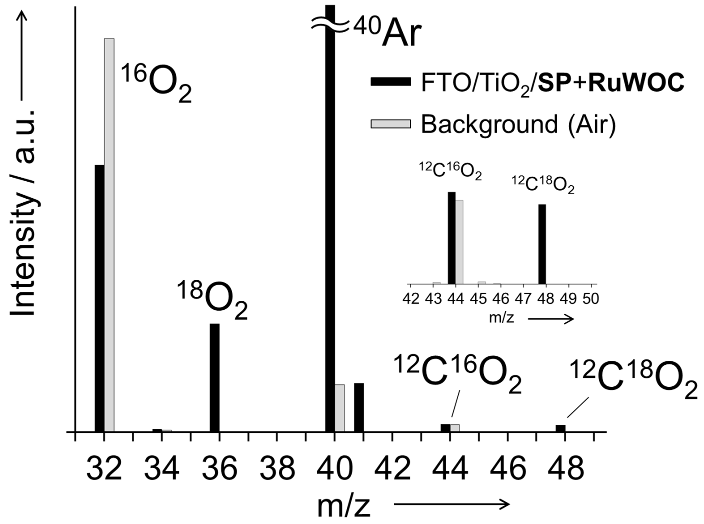

Figure S20. GC-MS of the photoelectrochemical products after 1 h of photolysis of 98 atom% $H_2{}^{18}O$ under white light illumination (λ_{ex} > 400 nm, 100 mW cm^{-2}) using the FTO/TiO$_2$/**SP**+**RuWOC** photoanode (black) and background air (gray).

The background showed almost no $^{16}O^{18}O$ (0.2%) and $^{18}O_2$ (0.0004%) peaks, whereas the gas fraction from the photoanode compartment after the photolysis of $H_2{}^{18}O$ using the FTO/TiO$_2$/**SP**+**RuWOC** as the photoanode revealed remarkable evolution of $^{18}O_2$ (Figure S19). ^{18}O-lableled CO$_2$ (Mw = 48) was also detected, indicating the oxidative degradation of **SP** and **RuWOC** on the surfaces with $H_2{}^{18}O$ as an oxygen source.[S12] The oxidative degradation explains the nonunit Faradaic efficiency of the photoanodic reactions.

S14. Catalytic Turnover

The $^{18}O_2$ evolution by the photoelectrochemical $H_2{}^{18}O$ oxidation using visible light was confirmed by GC-MS analysis (Figure 4a and S19); therefore, we determined the catalytic turnover in the photoelectrochemical conversion of water to O_2. The integrated charge over 1 h of white light irradiation was 20.0 mC, and the GC analysis revealed that 33 nmol of O_2 was evolved. The Faradaic efficiency was determined as follows:

$$\text{Faradaic Efficiency} = \frac{4 \times n_{\mathrm{O_2}}}{Q} = \frac{4 \times 33\ [\mathrm{nmol}]}{\frac{20.0 \times 10^{-3}\ [\mathrm{A \cdot s}]}{96485\ [\mathrm{A \cdot s/mol}]}} = 64\%$$

The catalyst loading onto the FTO/TiO_2 electrode is $(3.2 \pm 0.6) \times 10^{-9}$ mol cm^{-2} according to the optical analysis and Equation S1, and the active area for the photoelectrochemical analysis was 0.38 cm^2. The TON is determined as follow:

$$\text{TON} = \frac{n_{\mathrm{O_2}}}{n_{\mathrm{RuWOC}}} = \frac{33\ [\mathrm{mol}]}{3.2 \times 10^{-9} [\mathrm{mol/cm^2}] \times 0.38\ [\mathrm{cm^2}]} = 27$$

The TON was divided by 60 min to provide the average turnover frequency (TOF$_{\mathrm{ave}}$): 0.45 min^{-1}.

Considering the O_2 liberation rate from Ru$^{\mathrm{IV}}$−OO−Ru$^{\mathrm{IV}}$ species during heterogeneous Ru-bda-catalyzed water oxidation, 5.8 s^{-1},[S13] and the surface loading of the catalyst, 3.2×10^{-9} mol cm^{-2}, a maximum current density of 7.2 mA cm^{-2} was expected for the electrochemical and photoelectrochemical water oxidation. However, the obtained steady current was at most 60 μA cm^{-2} under white light illumination ($\lambda_{\mathrm{ex}} > 420$ nm, 100 mW cm^{-2}). If the rate-determining step is the intermolecular ET reaction, the rate would be 3.8×10^{-2} s^{-1}.

S15. Spectroelectrochemistry for the Assignment of SP$^{•+}$ Radical Cation

Spectroelectrochemical measurements were performed using an ALS660A electrochemical analyzer and a three-electrode electrochemical cell with the FTO/TiO_2/**SP** working electrode, the Pt wire counter electrode, and a Ag/$AgNO_3$ reference electrode with a Lambda 900 (Perkin-Elmer) UV/vis/NIR spectrometer. The absorption spectra of the electrode before and after the spectroelectrochemical measurements remained almost the same.

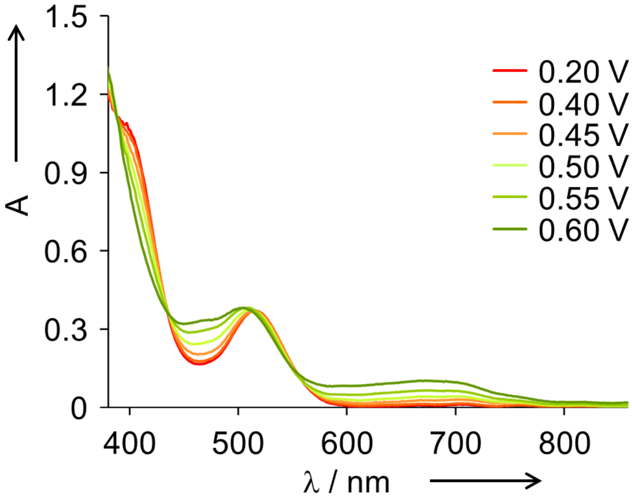

Figure S21. Change in the absorption spectra of the FTO/TiO_2/**SP** electrode during electrochemical oxidation at an applied potential of 0.20 − 0.60 V vs Ag/$AgNO_3$ in CH_2Cl_2 containing 0.1 M of $TBAPF_6$. The TiO_2 electrodes were prepared by screen printing techniques, and the TiO_2 thickness was 2 μm.

S16. Transient Absorption of SP in Solution and SP Adsorbed to TiO_2 Electrodes (with and without RuWOC)

TA measurements were carried out using a home-built pump-probe setup. Laser pulses (800 nm, 80 fs pulse length, 1 kHz repetition rate) were generated by a regenerative amplifier (Spitfire XP Pro) seeded by a femtosecond oscillator (MaiTai, both Spectra Physics). Excitation pulses at the wavelength of 530 nm were acquired using an optical parametric amplifier (Topas C, Light Conversion). The maximum used excitation photon flux was 9×10^{14} photons/cm^2/pulse. The probe, a broad supercontinuum spectrum, was generated by the 800-nm fundamental beam focused in a CaF_2 plate and split by a beam splitter into a probe and a reference beams. The probe and the reference beam were then dispersed in a spectrograph and detected by a double diode array (Pascher Instruments). To avoid photodegradation, the films were automatically shifted to a fresh spot after each kinetic scan. Maximum measurable delay in the femtosecond setup is determined by the optical length of a delay stage, which is 10 ns in this case (1.5 m, double pass).

For recording the μs dynamics an externally triggered Q-switched Nd: YVO4 laser (Advanced Optical Technology, 532 nm, 1 ns pulses) was used as a pump source, while the ordinary femtosecond detection with supercontinuum probe was used to record the transient changes in the absorption. The experimental conditions were very similar as for the femtosecond measurements.

SP in solution and **SP** adsorbed to TiO_2 electrodes (with and without RuWOC) were investigated on ultrafast and fast time scales, spanning from ~100 fs to 300 μs, probed by white-light continuum in the visible region. The transient spectra (Figure 5a) consist of four distinct spectral features – (i) **SP** singlet excited state in solution with strong ground state bleaching (GSB, negative signal) at 400 and 500 nm of the Soret-like and Q-like bands, respectively and broad positive excited-state absorption (ESA). The ESA is overlapped by stimulated emission (SE) of the **SP** (negative contribution at around 610 nm), matching the fluorescence spectrum (Figure S7). The singlet state (dashed line in Figure 5a) decays into a (ii) triplet spectrum when **SP** is in solution (Figure 5a, dash-dotted line) with ~ 4 ns lifetime, being consistent with that obtained from time-resolved fluorescence measurements (Figure S8). The **SP** triplet then decays single-exponentially back to the ground state with an ~1 μs time constant (kinetic in Figure S22).

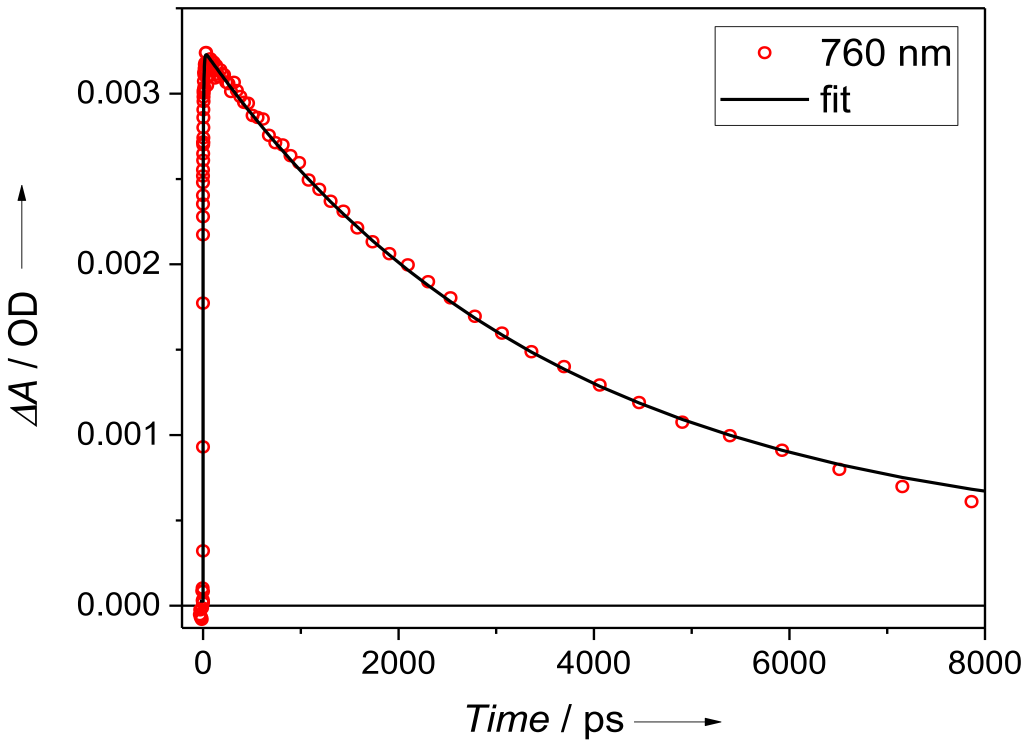

Figure S22. TA kinetic trace of **SP** in solution (at 760 nm) showing the decay of excited singlet state of **SP** into a triplet state (change of the spectrum (i) to (ii) in Figure 5a). The decay is in good agreement with time-correlated single photon counting of **SP** (Figure S8).

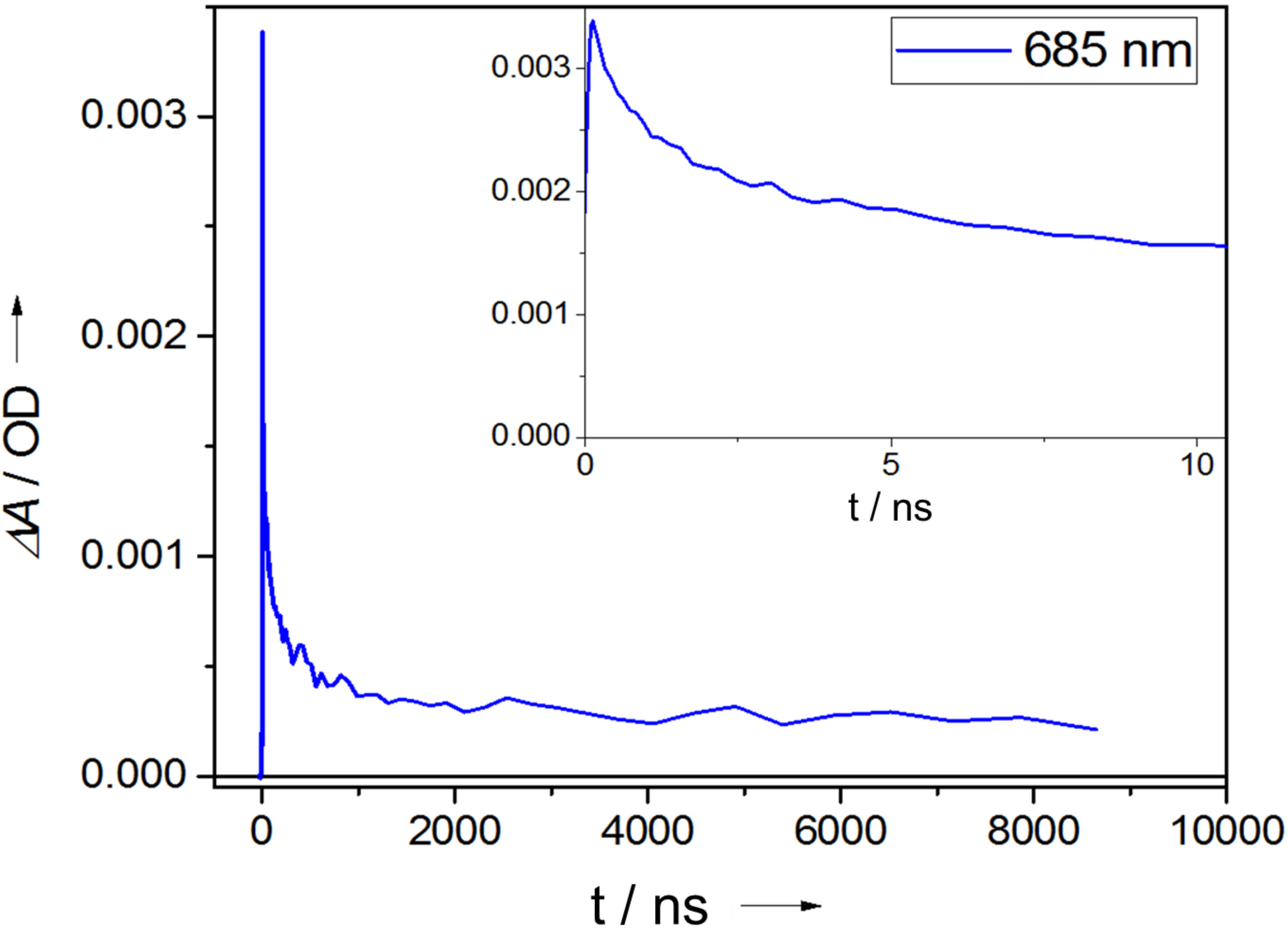

Figure S23. TA kinetic trace of **SP** on TiO_2 illustrating electron injection from **SP** to TiO_2. The kinetic at 685 nm shows the disappearance of the **SP** singlet state (spectrum (iii) in Figure 5a); the remaining, nondecaying signal is the oxidized dye (spectrum (iv) in Figure 5a).

S17. Fitting of the Time-dependent 2nd Order Reaction Dynamics

After the initial ultrafast electron injection (**SP**$^{\bullet+}$ formation), the fast decay (few ps to 300 μs) of the TiO_2/**SP** and TiO_2/**SP**+**RuWOC** electrodes is at best described by time-dependent 2nd order reaction dynamics. The fit is calculated as

$$\gamma_{(t)} = \frac{y_0}{t^{\alpha}}$$

and the results are in the **Table S1**, with t in μs. The γ is time-dependent 2nd order rate, expressed in Abs^{-1} μs^{-1} unit (since the molar extinction coefficient for $S^{\bullet+}$ and the thickness of the film are not known precisely under this conditions). Thus the rate at 1 μs is equal to the γ (1520 Abs^{-1}/μs for **SP** and 2810 Abs^{-1}/μs for **SP** + **RuWOC**). The α expresses how γ is changing with the time, thus if α would be equal to zero then the decay would be normal 2nd order reaction, but that is not the case here, however. This shows that (for the system measured) the recombination is driven by the hole diffusion as the hole "jumps" dye-to-dye towards the catalyst.

Table S1. Fit parameters for time-dependent 2nd order rate

System	γ	α
SP	1520	0.726
SP + **RuWOC**	2810	0.645

S18. References

S1. M. Yamamoto, L. Wang, F. Li, T. Fukushima, K. Tanaka, L. Sun and H. Imahori, *Chem. Sci.*, 2016, **7**, 1430−1439.

S2. L. Alibabaei, M. K. Brennaman, M. R. Norris, B. Kalanyan, W. J. Song, M. D. Losego, J. J. Concepcion, R. A. Binstead, G. N. Parsons and T. J. Meyer, *Proc. Natl. Acad. Sci. USA*, 2013, **110**, 20008−20013.

S3. M. W. Kanan and D. G. Nocera, *Science* 2008, **321**, 1072−1075.

S4. M. J. Frisch, G. W. Trucks, H. B. Schlegel, G. E. Scuseria, M. A. Robb, J. R. Cheeseman, J. A. Jr. Montgomery, T. Vreven, K. N. Kudin, J. C. Burant, J. M. Millam, S. S. Iyengar, J. Tomasi, V. Barone, B. Mennucci, M. Cossi, G. Scalmani, N. Rega, G. A. Petersson, H. Nakatsuji, M. Hada, M. Ehara, K. Toyota, R. Fukuda, J. Hasegawa, M. Ishida, T. Nakajima, Y. Honda, O. Kitao, H. Nakai, M. Klene, X. Li, J. E. Knox, H. P. Hratchian, J. B. Cross, V. Bakken, C. Adamo, J. Jaramillo, R. Gomperts, R. E. Stratmann, O. Yazyev, A. J. Austin, R. Cammi, C. Pomelli, J. W. Ochterski, P. Y. Ayala, K. Morokuma, G. A. Voth, P. Salvador, J. J. Dannenberg, V. G. Zakrzewski, S. Dapprich, A. D. Daniels, M. C. Strain, O. Farkas, D. K. Malick, A. D. Rabuck, K. Raghavachari, J. B. Foresman, J. V. Ortiz, Q. Cui, A. G. Baboul, S. Clifford, J. Cioslowski, B. B. Stefanov, G. Liu, A. Liashenko, P. Piskorz, I. Komaromi, R. L. Martin, D. J. Fox, T. Keith, M. A. Al-Laham, C. Y. Peng, A. Nanayakkara, M. Challacombe, P. M. W. Gill, B. Johnson, W. Chen, M. W. Wong, C. Gonzalez and J. A. Pople, *Gaussian 03*, Revision C.02; Gaussian, Inc.: Wallingford CT, 2004.

S5. (a) R. López-Arteaga, A. B. Stephansen, C. A. Guarin, T. I. Sølling and J. Peon, *J. Phys. Chem. C*, 2013, **117**, 9947−9955; (b) E. Collado-Fregoso, J. S. Zugazagoitia, E. F. Plaza-Medina and J. Peon, *J. Phys. Chem. C*, 2009, **113**, 134980−13508.

S6. F. Li, K. Fan, L. Wang, Q. Daniel, L. Duan and L. Sun, *ACS Catal.*, 2015, **5**, 3786−3790.

S7. E. Tsurumaki, S. Saito, K. S. Kim, J. M. Lim, Y. Inokuma, D. Kim and A. Osuka, *J. Am. Chem. Soc.*, 2008, **130**, 438−439.

S8. E. Tsurumaki, Y. Inokuma, S. Easwaramoorthi, J. M. Lim, D. Kim and A. Osuka, *Chem. Eur. J.*, 2009, **15**, 237−247.

S9. E. Tsurumaki, J. Sun, D. Kim and A. Osuka, *J. Am. Chem. Soc.*, 2015, **137**, 1056−1059.

S10. W.-Y. Cha, J. M. Lim, K. H. Park, M. Kitano, A. Osuka and D. Kim, *Chem. Commun.*, 2014, **50**, 8491−8494.

S11. Z. Chen, J. J. Concepcion, J. W. Jurss and T. J. Meyer, *J. Am. Chem. Soc.*, 2009, **131**, 15580−15581.

S12. (a) K.-R. Wee, B. D. Sherman, M. K. Brennaman, M. V. Sheridan, A. Nayak, L. Alibabaei and T. J. Meyer, *J. Mater. Chem. A*, 2016, **4**, 2969−2975; (b) J. T. Hyde, K. Hanson, A. K. Vannucci, A. M. Lapides, L. Alibabaei, M. R. Norris, T. J. Meyer and D. P. Harrison, *ACS Appl. Mater. Interfaces*, 2015, **7**, 9554−9562.

S13. L. Duan, F. Bozoglian, S. Mandal, B. Stewart, T. Privalov, A. Llobet and L. Sun, *Nat. Chem.*, 2012, **4**, 418−423.

S14. L. Wang, M. Mirmohades, A. Brown, L. Duan, F. Li, Q. Daniel, R. Lomoth, L. Sun and L. Hammarström, *Inorg. Chem.*, 2015, **54**, 2742−2751.